Thermally Driven Electronic Topological Transition in FeTi

F. C. Yang,[1] J. A. Muñoz,[1,2] O. Hellman,[1] L. Mauger,[1] M. S. Lucas,[1,3] S. J. Tracy,[1] M. B. Stone,[4] D. L. Abernathy,[4] Yuming Xiao,[5] and B. Fultz[1]

[1]*Applied Physics and Materials Science, California Institute of Technology, Pasadena, California 91125, USA*
[2]*The Datum Institute, Beaverton, Oregon 97005, USA*
[3]*Air Force Research Laboratory, Wright-Patterson AFB, Ohio 45433, USA*
[4]*Quantum Condensed Matter Division, Oak Ridge National Laboratory, Oak Ridge, Tennessee 37831, USA*
[5]*HPCAT, Geophysical Laboratory, Carnegie Institution of Washington, Argonne, Illinois 60439, USA*

(Received 22 March 2016; published 8 August 2016)

Ab initio molecular dynamics, supported by inelastic neutron scattering and nuclear resonant inelastic x-ray scattering, showed an anomalous thermal softening of the M_5^- phonon mode in $B2$-ordered FeTi that could not be explained by phonon-phonon interactions or electron-phonon interactions calculated at low temperatures. A computational investigation showed that the Fermi surface undergoes a novel thermally driven electronic topological transition, in which new features of the Fermi surface arise at elevated temperatures. The thermally induced electronic topological transition causes an increased electronic screening for the atom displacements in the M_5^- phonon mode and an adiabatic electron-phonon interaction with an unusual temperature dependence.

DOI: 10.1103/PhysRevLett.117.076402

An electronic topological transition (ETT), first identified by Lifshitz [1], occurs when changes to a metal cause new features to appear in the topology of the Fermi surface [2]. Structural, mechanical, and electronic properties are usually altered by an ETT, which can be induced by alloying [3–5] or pressure [6–8]. Recently a novel temperature-induced ETT has been reported to alter magnetoresistivity [9]. In this Letter, we show through first-principles calculations and ancillary experiments how a thermally driven ETT drives anomalous changes in phonon dynamics.

FeTi is a thermodynamically stable [10–12] nonmagnetic [13] intermetallic compound with a bcc-based $B2$ structure and a melting point of approximately 1600 K. FeTi is of interest for its hydrogen absorption capabilities [14–16] and for its mechanical properties [17,18]. It has been the subject of a large number of experimental and theoretical studies including inelastic neutron scattering [19,20] and first-principles calculations [21–23]. The calculations show that FeTi has a Fermi level that lies in a pseudogap in its electronic density of states (DOS) [24–26], so thermal smearing could increase the effective density of electrons at the Fermi level.

First-principles calculations on FeTi were performed with projector-augmented wave potentials [27,28] and the generalized gradient approximation [29] of density functional theory (DFT) [30] using the VASP package [31,32]. The electronic DOS curves at various temperatures were obtained through static calculations and constant volume *ab initio* molecular dynamics (AIMD) calculations on 128-atom supercells. Convergence with respect to kinetic energy cutoffs and sampling of k points in the Brillouin zone was checked in all cases. The calculations show that the pseudogap is present at the Fermi level in the 0 K electronic DOS, and is filled as the number of electronic states at the Fermi level increases by 218% from 0 to 1035 K, as shown in the Supplemental Material [33].

Forces and atomic configurations in the AIMD simulations were used to compute phonon energies at different temperatures with the temperature-dependent effective potential (TDEP) method [47,48], in which a model Hamiltonian

$$\hat{H} = U_0 + \sum_i \frac{\mathbf{p}_i^2}{2m_i} + \frac{1}{2}\sum_{ij} \mathbf{u}_i \bar{\bar{\Phi}}_{ij} \mathbf{u}_j, \tag{1}$$

is used to sample the potential energy surface at the most probable atom positions, where $\mathbf{p}_i$ and $\mathbf{u}_i$ are the momentum and displacement of atom i, respectively, and $\bar{\bar{\Phi}}_{ij}$ is a second-order force constant matrix. The force constants from Eq. (1) were used to obtain phonon dispersions and phonon DOS curves at temperatures from 300 to 1500 K (Fig. 1). Thermal expansion causes phonons to soften with temperature, and this was accounted for by the quasiharmonic calculations presented in the Supplemental Material [33]. The AIMD calculations were performed without thermal expansion, so Fig. 1 shows the thermal effects from pure anharmonicity and from the adiabatic EPI. These are significantly larger than the thermal softenings from quasiharmonicity reported in the Supplemental Material [33].

The nonadiabatic electron-phonon interaction (EPI) is well known from conventional superconductivity, where electrons are paired by phonons with wave vectors that span the Fermi surface [49,50]. With increasing temperature the

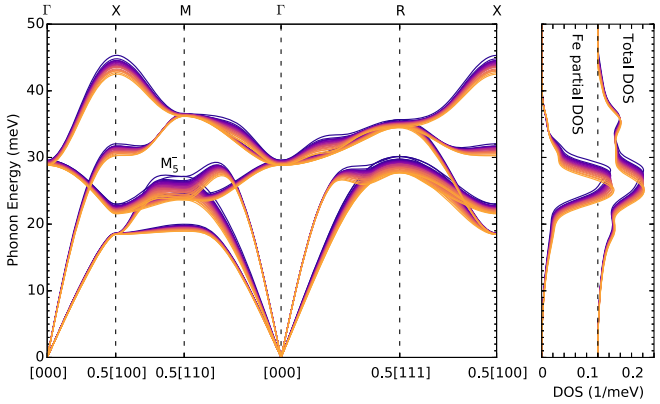

FIG. 1. Calculated FeTi phonon dispersions at temperatures from 300 to 1500 K. Also shown are phonon DOS curves for the motions of all atoms (total) and iron atoms (Fe partial).

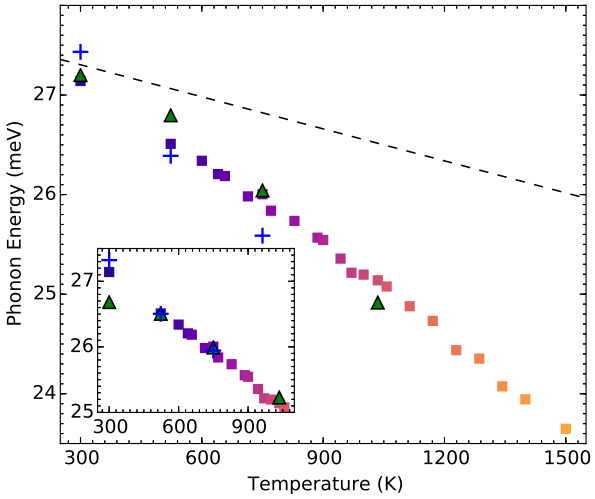

FIG. 2. Temperature dependence of the M_5^- phonon energy calculated from TDEP (squares). The colors of the squares are identical to those shown in Fig. 1. The green and blue markers are mean phonon energies obtained from Lorentizan fits to the Fe nuclear-resonant inelastic x-ray scattering (NRIXS) DOS and the inelastic neutron scattering (INS) DOS, respectively. The dashed line is the thermal softening of the M_5^- phonon from quasiharmonicity alone. The inset shows the agreement in the slopes of the experimental and computational phonon energies without quasiharmonic contributions. For convenience in showing the slopes, the NRIXS data were offset by −0.76 meV and the INS by −0.35 meV.

effects of the nonadiabatic EPI dissipate [49], but there can be an increase in the adiabatic EPI, which requires excitations of both electrons and phonons [51,52]. The adiabatic EPI can have a significant effect on the high-temperature thermodynamics of materials with sharp features in the electronic DOS at the Fermi level because the thermal broadening of electronic states can change the availability of electrons to screen atomic displacements in phonons [53–56].

To help understand the EPI in FeTi, density functional perturbation theory [57] implemented with the Quantum ESPRESSO package [58] was used to calculate 0 K electron-phonon linewidths

$$\Gamma_{\mathbf{q}\nu} = \frac{4\pi}{N_k}\sum_{\mathbf{k}mn}|g^{\nu}_{mn}(\mathbf{k},\mathbf{q})|^2(f_{\mathbf{k}m} - f_{\mathbf{k}+\mathbf{q}n}) \times \delta(\hbar\omega_{\mathbf{q}\nu} + \varepsilon_{\mathbf{k}m} - \varepsilon_{\mathbf{k}+\mathbf{q}n}), \quad (2)$$

where $g^{\nu}_{mn}(\mathbf{k},\mathbf{q})$ is the matrix element of an EPI involving a phonon and two electrons with respective wave vector and band indices $\mathbf{k}m$ and $\mathbf{k}+\mathbf{q}n$, $f_{\mathbf{k}m}$ is the Fermi-Dirac distribution for electrons, and $\varepsilon_{\mathbf{k}m}$ is the eigenenergy of an electron. The Supplemental Material shows that many of the modes that soften with temperature in Fig. 1 are those with strong electron-phonon coupling and large $\Gamma_{\mathbf{q}\nu}$ [33]. Interestingly, these calculations showed that the M_5^- mode has a negligible electron-phonon linewidth at 0 K, even though it shows the strongest thermal softening in Fig. 1.

Figure 1 shows the anomalous behavior of the M_5^- mode, which softens increasingly rapidly with temperature as shown in Fig. 2. The M_5^- mode and modes near it contribute strongly to the softening of the phonon DOS peak around 25–27 meV. This mode is dominated by the motions of iron atoms, and both the experimental DOS curves from INS and NRIXS shown in Fig. 3 emphasize phonon scattering from iron atoms (Ti is a weaker scatterer of neutrons, and Ti cannot contribute to the NRIXS spectrum). When the phonon softening from thermal expansion, obtained from quasiharmonic calculations described in the Supplemental Material [33], is removed from the experimental points, the agreement in slopes of the curves in Fig. 2 is excellent. The magnitudes of the phonon energies show agreement between computation and experiment that is better than expected. For example, the experimental peaks include

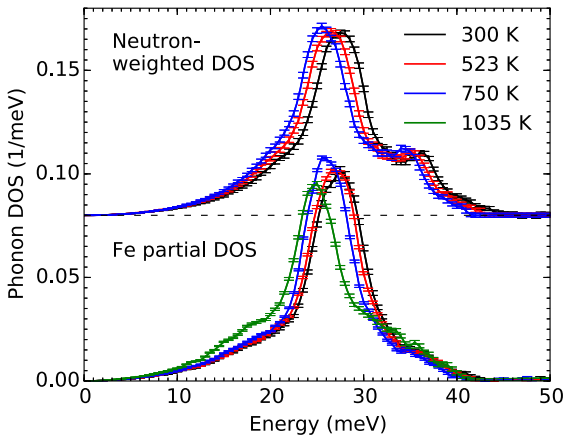

FIG. 3. Experimental FeTi phonon DOS curves. The neutron-weighted DOS curves were obtained from INS measurements and the Fe partial DOS curves from NRIXS measurements. Error bars are from counting statistics.

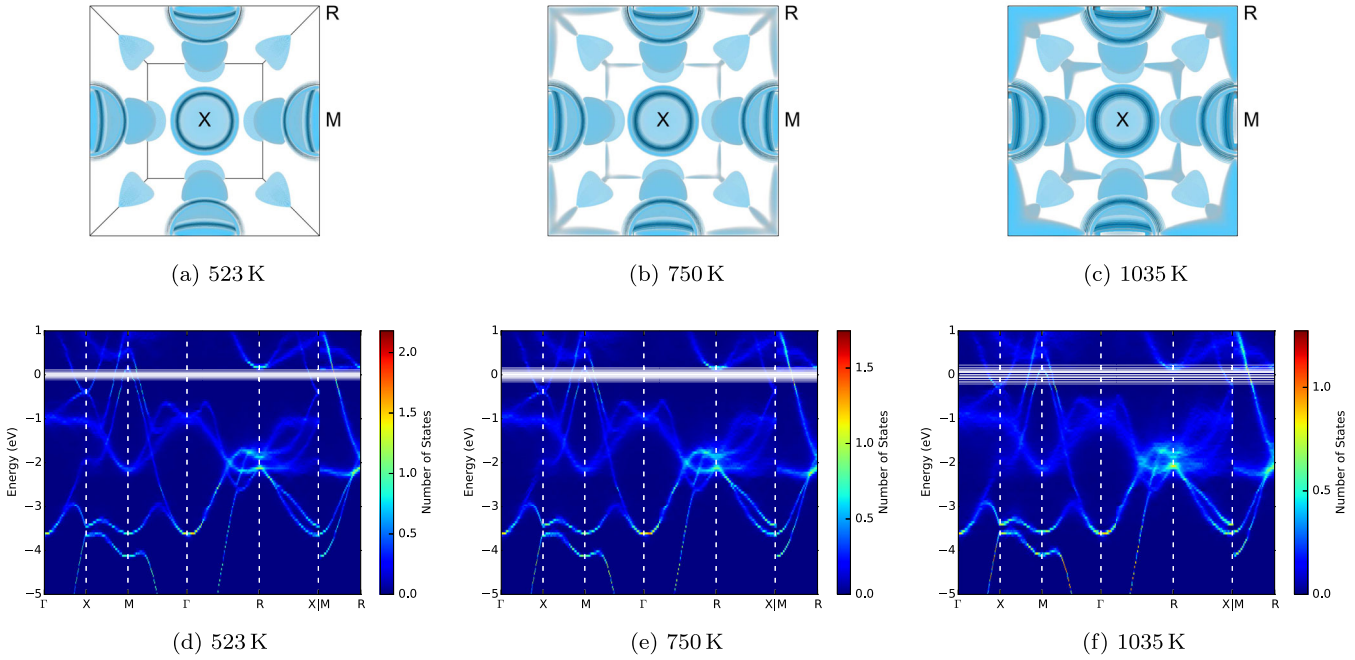

(a) 523 K (b) 750 K (c) 1035 K

(d) 523 K (e) 750 K (f) 1035 K

FIG. 4. (a)–(c) Approximated finite-temperature Fermi surfaces in the Brillouin zone: (a) 523 K, (b) 750 K, and (c) 1035 K. The dark blue surfaces are the unshifted 0 K Fermi surfaces, and the lighter blue surfaces are at energies shifted from the Fermi energy by factors of $1.8k_BT$. (d)–(f) Finite-temperature band structures from supercell AIMD calculations, produced by BANDUP [59,60]: (d) 523 K, (e) 750 K, and (f) 1035 K. The Fermi surface and band structure at 523 K resemble those at 0 K without any broadening.

contributions from phonons around the R point, which lie above 3 meV higher than the M_5^- mode. (Agreement at lower temperatures is not expected owing to the use of classical statistical mechanics in the AIMD calculations.)

To calculate the adiabatic EPI, the effects of phonons were simulated by DFT calculations on supercells with thermal atom displacements, obtained at random times during the AIMD simulations. The thermal excitations of electrons were described by a thermal smearing function from the energy derivative of the Fermi-Dirac distribution function, which is similar to a Gaussian function with a standard deviation of $\sigma = 1.8k_BT$. A discrete set of energies representative of this thermal spread gave a set of Fermi levels that were used to construct the Fermi surfaces of Figs. 4(a)–(c). The BANDUP code [59,60] was used to project the supercell band structures into the range of k-space for a standard $B2$ unit cell. Through unfolding operations [61], BANDUP obtains effective primitive cell representations of the band structures of systems simulated using supercells. Results are shown in Figs. 4(d)–(f). (We found no noticeable differences in the band structures when thermal expansion was included, as reported previously in Ref. [23].)

Owing to a decrease in band energy from thermal atom displacements, but more to the thermal smearing of the Fermi level, electronic states at the R point that lie above the Fermi level at 0 K intersect the Fermi level at high temperatures. New topological features appear in the Fermi surface around the R symmetry points and along the M–R symmetry lines of the Brillouin zone, as shown in Figs. 4(a)–(c). These new features grow with increasing temperature. This is a thermally driven electronic topological transition.

When the Fermi surface allows for many spanning vectors of phonons, the electronic screening of charge displacements can be more efficient, and phonons exhibit softenings such as Kohn anomalies [62]. With the appearance of thermally driven features of the Fermi surface around the R point, new sets of spanning vectors are available to couple electronic states across the Fermi surface. Spanning vectors along the $[\xi\xi 0]$ and $[\frac{1}{2}\xi 0]$ directions that connect these new features and the Fermi surface feature around the X points were counted as described in the Supplemental Material [33]. The numbers of vectors obtained for 1035 K are displayed in a histogram in Fig. 5. This distribution overlaps well with the group of wave vectors over which the TA and LA phonon branches soften significantly around the M symmetry point. These new spanning vectors should increase screening of the corresponding phonon modes by conduction electrons, causing the large softening of phonons as seen in Fig. 2. The softening graphed in Fig. 5 was corrected for the softening expected from phonon-phonon interactions calculated by the TDEP method, as described in the Supplemental Material [33].

Interatomic force constants were calculated by the TDEP method, and they showed thermal weakening of both Fe–Ti first-nearest-neighbor (1NN) transverse force constants and

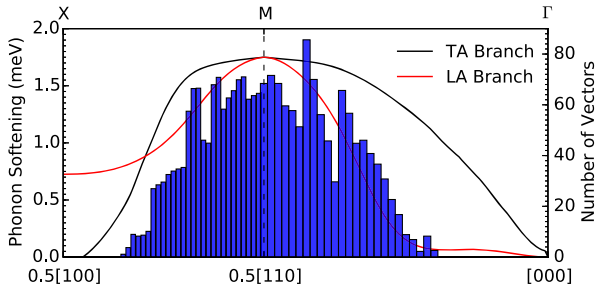

FIG. 5. Histogram of spanning vectors that couple the new states at one of the R symmetry points with the rest of the Fermi surface along the $[\xi\xi 0]$ and $[\frac{1}{2}\xi 0]$ directions at 1035 K, displayed together with the changes in energies of the transverse acoustic (TA) and longitudinal acoustic (LA) branches from 300 to 1035 K along the same directions.

Fe–Fe second-nearest-neighbor (2NN) longitudinal force constants. By testing the sensitivity of the phonon dispersions to changes in these force constants, we found that the thermal weakening of both the Fe–Ti 1NN transverse force constants and the Fe–Fe 2NN longitudinal force constants contribute significantly to the thermal softening of the M_5^- mode. This behavior is consistent with the atomic displacement pattern shown in Fig. 6, in which (110) planes slide in opposite $[1\bar{1}0]$ directions. (This is also a proposed displacement pattern for the structural phase transition in $B2$-ordered NiTi, a shape-memory alloy [63,64].) From the phonon polarization vectors, we found that the magnitude of the Fe displacement is at least twice as that of Ti. Softening of the Fe–Ti 1NN transverse force constants and the Fe–Fe 2NN longitudinal force constants are particularly effective for softening the M_5^- mode, and these changes occur with the thermally driven ETT.

It has been known for a number of years that the adiabatic EPI can alter the phonon dynamics, often making an important contribution to the free energy of a metal or alloy. A temperature dependence of the adiabatic EPI occurs when there is a substantial variation in the electronic

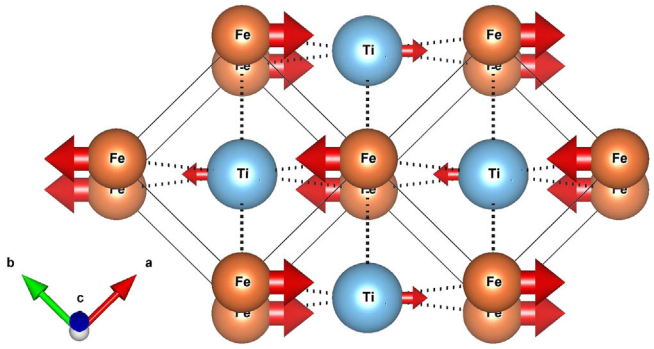

FIG. 6. A view of the displacement pattern of the M_5^- phonon, in which Fe (orange) and Ti (blue) atoms move along the $[1\bar{1}0]$ directions. The dashed lines are the 1NN Fe–Ti interactions, and the solid lines are the 2NN Fe–Fe interactions.

DOS at the Fermi level, for example. A thermally driven ETT is expected to cause more rapid and perhaps more abrupt changes with temperature. Such effects are expected in materials with occupied or unoccupied bands that are a few k_BT away from the Fermi level at low temperatures, so these effects are expected in many systems. Shifts and broadenings of the electronic bands from atomic displacement disorder can enhance or diminish these effects.

This work was supported by the Department of Energy through the Basic Energy Sciences Grant No. DE-FG02-03ER46055. The portions of this work conducted at Oak Ridge National Laboratory were supported by the Scientific User Facilities Division and by the Division of Materials Sciences and Engineering, Office of Basic Energy Sciences, DOE. Portions of this work were performed at HPCAT (Sector 16), Advanced Photon Source (APS), Argonne National Laboratory. HPCAT is supported by CIW, CDAC, UNLV, and LLNL through funding from DOE-NNSA, DOE-BES, and NSF. APS is supported by DOE-BES, under Contract No. DE-AC02-06CH11357. This work benefited from DANSE software developed under NSF Grant No. DMR-0520547. Supercomputer resources were provided by the Swedish National Infrastructure for Computing (SNIC).

[1] I. M. Lifshitz, Zh. Eksp. Teor. Fiz. **38** (1960) [Sov. Phys. JETP **11**, 1130 (1960)].
[2] Y. M. Blanter, M. I. Kaganov, A. V. Pantsulaya, and A. A. Varlamov, Phys. Rep. **245**, 159 (1994).
[3] E. Bruno, B. Ginatempo, E. S. Guiliano, A. V. Ruban, and Y. K. Vekilov, Phys. Rep. **249**, 353 (1994).
[4] V. G. Vaks and A. V. Trefilov, J. Phys. F **18**, 213 (1988).
[5] V. G. Vaks and A. V. Trefilov, J. Phys. Condens. Matter **3**, 1389 (1991).
[6] S. L. Bud'ko, A. N. Voronovskii, A. G. Gapotechenko, and E. S. Itskevich, Zh. Eksp. Teor. Fiz. **86**, 778 (1984) [Sov. Phys. JETP **59**, 454 (1984)].
[7] A. F. Goncharov and V. V. Struzhkin, Physica (Amsterdam) **385C**, 117 (2003).
[8] A. Polian, M. Gauthier, S. M. Souza, D. M. Trichês, J. Cardoso de Lima, and T. A. Grandi, Phys. Rev. B **83**, 113106 (2011).
[9] Y. Wu, N. H. Jo, M. Ochi, L. Huang, D. Mou, S. L. Bud'ko, P. C. Canfield, N. Trivedi, R. Arita, and A. Kaminski, Phys. Rev. Lett. **115**, 166602 (2015).
[10] J. L. Murray, *Phase Diagrams of Binary Titanium Alloys* (ASM International, Metals Park, 1987).
[11] H. Ohtani, N. Hanaya, M. Hasebe, S. I. Teraoka, and M. Abe, CALPHAD: Comput. Coupling Phase Diagrams Thermochem. **30**, 147 (2006).
[12] L.-F. Zhu, M. Friák, A. Dick, B. Grabowski, T. Hickel, F. Liot, D. Holec, A. Schlieter, U. Kün, J. Eckert, Z. Ebrahumi, H. Emmerich, and J. Neugebauer, Acta Mater. **60**, 1594 (2012).
[13] M. V. Nevitt, J. Appl. Phys. **31**, 155 (1960).

[14] J. J. Reilly and R. H. Wiswall, Jr., Inorg. Chem. **13**, 218 (1974).
[15] B. Sakintuna, F. Lamari-Darkrim, and M. Hirscher, Int. J. Hydrogen Energy **32**, 1121 (2007).
[16] L. Zaluski, A. Zaluska, P. Tessier, J. O. Ström-Olsen, and R. Schulz, J. Alloys Compd. **227**, 53 (1995).
[17] J. Das, K. B. Kim, F. Baier, W. Löser, and J. Eckert, Appl. Phys. Lett. **87**, 161907 (2005).
[18] J. Das, K. B. Kim, F. Baier, W. Löser, A. Gebert, and J. Eckert, J. Alloys Compd. **434–435**, 28 (2007).
[19] S. M. Shapiro, F. Reidinger, and J. R. Lynch, J. Phys. F **12**, 1869 (1982).
[20] U. Buchenau, H. R. Schober, J.-M. Welter, G. Arnold, and R. Wagner, Phys. Rev. B **27**, 955 (1983).
[21] J. Yamashita and S. Asano, Prog. Theor. Phys. **48**, 2119 (1972).
[22] D. A. Papaconstantopoulos, Phys. Rev. B **11**, 4801 (1975).
[23] L.-F. Zhu, M. Friák, A. Udyansky, D. Ma, A. Schlieter, U. Kühn, J. Eckert, and J. Neugebauer, Intermetallics **45**, 11 (2014).
[24] R. Eibler, J. Redinger, and A. Neckel, J. Phys. F **17**, 1533 (1987).
[25] J. Y. Rhee, B. N. Harmon, and D. W. Lynch, Phys. Rev. B **54**, 17385 (1996).
[26] A. Kellou, Z. Nabi, A. Tadjer, N. Amrane, N. Fenineche, and H. Aourag, Phys. Status Solidi (b) **239**, 389 (2003).
[27] P. E. Blöchl, Phys. Rev. B **41**, 5414 (1990).
[28] G. Kresse and D. Joubert, Phys. Rev. B **59**, 1758 (1999).
[29] J. P. Perdew, K. Burke, and M. Ernzerhof, Phys. Rev. Lett. **77**, 3865 (1996).
[30] W. Kohn and L. J. Sham, Phys. Rev. **140**, A1133 (1965).
[31] G. Kresse and J. Furthmüller, Phys. Rev. B **54**, 11169 (1996).
[32] G. Kresse and J. Furthmüller, Comput. Mater. Sci. **6**, 15 (1996).
[33] See Supplemental Material, which includes Refs. [34–46], at http://link.aps.org/supplemental/10.1103/PhysRevLett.117.076402 for technical details of the experiments and calculations and additional calculations of the phonon softening from thermal expansion, the electron-phonon linewidths, the electronic density of states, and the phonon dispersions.
[34] W. Sturhahn, Hyperfine Interact. **125**, 149 (2000).
[35] D. L. Abernathy, M. B. Stone, M. J. Loguillo, M. S. Lucas, O. Delaire, X. Tang, J. Y. Y. Lin, and B. Fultz, Rev. Sci. Instrum. **83**, 015114 (2012).
[36] B. Fultz, T. Kelley, J. Lin, J. Lee, O. Delaire, M. Kresch, M. McKerns, and M. Aivazis, *Experimental Inelastic Neutron Scattering: Introduction to* DANSE, http://www.its.caltech.edu/~matsci/btfgrp/Inelastic_Neutron_Book.pdf.
[37] M. S. Lucas, J. A. Muñoz, O. Delaire, N. D. Markovskiy, M. B. Stone, D. L. Abernathy, I. Halevy, L. Mauger, J. B. Keith, M. L. Winterrose, Y. Xiao, M. Lerche, and B. Fultz, Phys. Rev. B **82**, 144306 (2010).
[38] J. A. Muñoz, M. S. Lucas, O. Delaire, M. L. Winterrose, L. Mauger, C. W. Li, A. O. Sheets, M. B. Stone, D. L. Abernathy, Y. Xiao, P. Chow, and B. Fultz, Phys. Rev. Lett. **107**, 115501 (2011).
[39] J. A. Muñoz, M. S. Lucas, L. Mauger, I. Halevy, J. Horwath, S. L. Semiatin, Y. Xiao, P. Chow, M. B. Stone, D. L. Abernathy, and B. Fultz, Phys. Rev. B **87**, 014301 (2013).
[40] J. A. Muñoz, Ph.D. thesis, California Institute of Technology, 2013.
[41] H. J. Monkhorst and J. D. Pack, Phys. Rev. B **13**, 5188 (1976).
[42] K. Parlinski, Z-.Q. Li, and Y. Kawazoe, Phys. Rev. Lett. **78**, 4063 (1997).
[43] A. Togo, F. Oba, and I. Tanaka, Phys. Rev. B **78**, 134106 (2008).
[44] D. Vanderbilt, Phys. Rev. B **41**, 7892 (1990).
[45] S. Nosé, J. Chem. Phys. **81**, 511 (1984).
[46] A. A. Maradudin and A. E. Fein, Phys. Rev. **128**, 2589 (1962).
[47] O. Hellman, I. A. Abrikosov, and S. I. Simak, Phys. Rev. B **84**, 180301 (2011).
[48] O. Hellman, P. Steneteg, I. A. Abrikosov, and S. I. Simak, Phys. Rev. B **87**, 104111 (2013).
[49] G. Grimvall, *The Electron-Phonon Interaction in Metals* (North-Holland, Amsterdam, 1981).
[50] J. Bardeen, L. N. Cooper, and J. R. Schrieffer, Phys. Rev. **108**, 1175 (1957).
[51] N. Bock, D. Coffey, and D. C. Wallace, Phys. Rev. B **72**, 155120 (2005).
[52] N. Bock, D. C. Wallace, and D. Coffey, Phys. Rev. B **73**, 075114 (2006).
[53] O. Delaire, M. Kresch, J. A. Muńoz, M. S. Lucas, J. Y. Y. Lin, and B. Fultz, Phys. Rev. B **77**, 214112 (2008).
[54] O. Delaire, M. S. Lucas, J. A. Muñoz, M. Kresch, and B. Fultz, Phys. Rev. Lett. **101**, 105504 (2008).
[55] O. Delaire, K. Marty, M. B. Stone, P. R. C. Kent, M. S. Lucas, D. L. Abernathy, D. Mandrus, and B. C. Sales, Proc. Natl. Acad. Sci. U.S.A. **108**, 4725 (2011).
[56] B. Fultz, Prog. Mater. Sci. **55**, 247 (2010).
[57] S. Baroni, S. de Gironcoli, A. Dal Corso, and P. Giannozzi, Rev. Mod. Phys. **73**, 515 (2001).
[58] P. Giannozzi *et al.*, J. Phys. Condens. Matter **21**, 395502 (2009).
[59] P. V. C. Medeiros, S. Stafström, and J. Björk, Phys. Rev. B **89**, 041407 (2014).
[60] P. V. C. Medeiros, S. S. Tsirkin, S. Stafström, and J. Björk, Phys. Rev. B **91**, 041116 (2015).
[61] V. Popescu and A. Zunger, Phys. Rev. B **85**, 085201 (2012).
[62] W. Kohn, Phys. Rev. Lett. **2**, 393 (1959).
[63] R. F. Hehemann and G. D. Sandrock, Scr. Metall. **5**, 801 (1971).
[64] X. Huang, C. Bungaro, V. Godlevsky, and K. M. Rabe, Phys. Rev. B **65**, 014108 (2001).